Metallurgy and Foundry Engineering – Vol. 41, 2015, No. 4, pp. 189–199
http://dx.doi.org/10.7494/mafe.2015.41.4.189

Hong Phong Nguyen, Tadeusz Niezgoda, Agnieszka Derewońko, Jerzy Jachimowicz

Numerical analysis of rod uniaxial tension considering thermo-mechanical coupling effect

Numeryczna analiza jednoosiowego rozciągania pręta z uwzględnieniem efektu sprzężenia termomechanicznego

Abstract
This paper presents numerical analyses of uniaxial tension tests on rods made of a material with elastic-plastic characteristics with mapping the temperature fields generated in the fields of plastic strains. The use of thermo-mechanical coupling algorithms implemented in CAE programs that enable us to enter the parameters of materials dependent on temperature and used to visualize the damage of the samples is presented. The numerical models were validated with experimental research.

Keywords: thermo-mechanical coupling, uniaxial tension, finite element method

Streszczenie
W pracy przedstawiono analizy numeryczne testów jednoosiowego rozciągania prętów wykonanych z materiału o charakterystyce sprężysto-plastycznej z odwzorowaniem pól temperatury generowanych w obszarach odkształceń trwałych. Zaprezentowano wykorzystanie algorytmów sprzężenia termomechanicznego zaimplementowanych w programach CAE, umożliwiających wprowadzenie parametrów materiałów zależnych od temperatury oraz stosowanych do wizualizacji zniszczenia próbek. Wyniki symulacji zwalidowano badaniami eksperymentalnymi.

Słowa kluczowe: sprzężenie termomechaniczne, jednoosiowe rozciąganie, metoda elementów skończonych

1. Introduction

As a structure is loaded with progressively increasing forces, there may occur areas of plastic strain. The work of forces on the corresponding displacements causes additional

Hong Phong Nguyen M.Sc. Eng., Tadeusz Niezgoda Ph.D. D.Sc. Eng., Agnieszka Derewońko Ph.D. Eng., Jerzy Jachimowicz Ph.D. Eng.: Military University of Technology, Faculty of Mechanical Engineering, Warsaw, Poland; hong.phong.nguyen@wat.edu.pl; agnieszka.derewonko@wat.edu.pl

heat inside the considered structure resulting from the processes occurring in the microstructure. The heat generated in the areas of permanent deformation affects the physical properties of the material from which the structure is made, such as yield strength and damage, thermal expansion, specific , or heat conductivity. In turn, weakening the strength properties of the structure causes enlargement of the areas of permanent deformation and, thereby, an increase in the amount of heat input and as consequences temperature in this area. This mutual dependence between the weakening of the strength properties caused by increasing temperature and the expansion of the area of permanent deformation resulted from what is called a result of thermo-mechanical coupling [1– 4].

The paper presents numerical analyses of uniaxial tensile tests on a sample using algorithms of thermo-mechanical coupling. The characteristics of physical properties dependent on temperature were introduced. Two cases of mapping the thermal boundary conditions were tested: one without thermal conditions and one with conduction of heat to the grips. The temperature fields generated in the uniaxial tensile test on a standard sample made of alloy steel for both cases are presented. The obtained results were compared with the results of the experiment. The compliance was satisfactory.

2. Theoretical basic

Numerical analyses were performed using LS-DYNA, to which the algorithm of thermo-mechanical coupling developed by Shapiro was implemented [5]. According to this algorithm, the differential equations of heat conduction are in the following form [6]:

$$\rho c_p \frac{\partial \theta}{\partial t} = \left(k_{ij} \theta_{,j} \right)_{,i} + Q \tag{1}$$

subject to boundary conditions, $\theta = \theta_{\Gamma_1}$ on Γ_1, $k_{ij}\theta_{,j}n_i + \beta\theta = \gamma$ on Γ_2, and initial condition at t_0 in volume of Ω (Fig. 1):

$$\theta_\Omega = \theta_0 \left(x_i \right) \text{ at } t = t_0 \tag{2}$$

where θ is temperature as a function of coordinates and time, x_i are coordinates as a function of time, ρ is density, c_p and k_{ij} represent specific heat, Q is an internal heat generation rate per unit volume in Ω, θ_{Γ_1} is temperature on Γ_1 and n_i is a normal vector to Γ_2. Equation (1) is solved by the finite element method.

In this study, the internal heat rate generated due to plastic deformation is calculated by the following formula:

$$Q = \eta \sigma_{ij} \dot{\varepsilon}_{ij}^p \tag{3}$$

where:

σ_{ij} – a stress tensor,
$\dot{\varepsilon}_{ij}$ – a plastic strain rate tensor,
η – fraction of plastic work converted into heat, which is equal to approximately 0.95 for most metals.

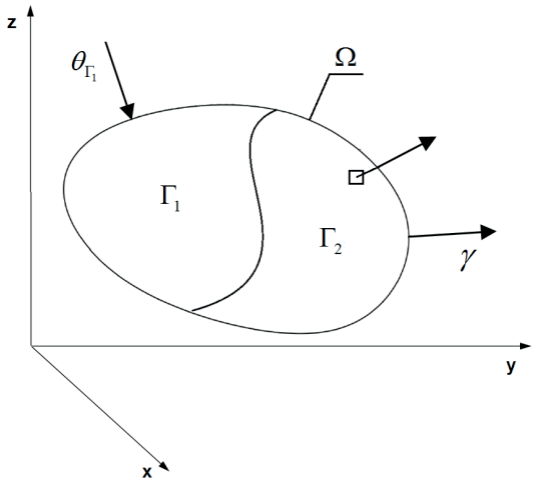

Fig. 1. Thermal boundary conditions

Thermal boundary conditions are given by

$$k_x \frac{\partial \theta}{\partial x} n_x + k_y \frac{\partial \theta}{\partial y} n_y + k_z \frac{\partial \theta}{\partial z} n_z = \gamma - \beta\theta = \dot{q}^n \tag{4}$$

To create the models, we used eight-node, hexahedral finite elements with linear shape functions. Newton's method is used to satisfy the equilibrium in nonlinear problems. Material properties are dependent on temperature and accounted for at the Gauss points.

An important feature for thermal-mechanical coupling analysis is the constitutive material model. Defining this model requires consideration of such phenomena as strain hardening, thermal softening, and thermal expansion caused by temperature. In this study, the thermo-elastic-plastic material model was used, as shown in Figure 2.

The yield condition is defined by

$$\varphi = \frac{1}{2} s_{ij} s_{ij} - \frac{\sigma_y^2(\theta)}{3} = 0 \tag{5}$$

where

$$s_{ij} = \sigma_{ij} - \frac{1}{3}\sigma_{kk}\delta_{ij} \tag{6}$$

$$\sigma_y(\theta) = \sigma_o(\theta) + E_p(\theta)\varepsilon_{eff}^p \tag{7}$$

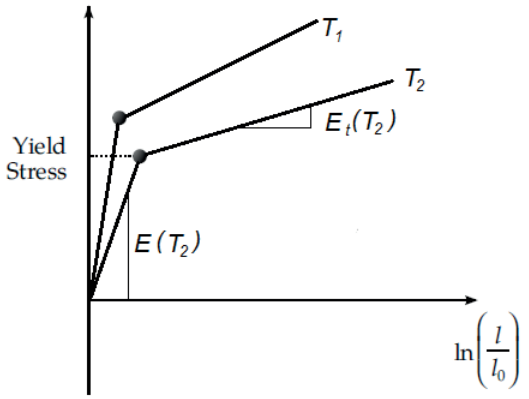

Fig. 2. Thermo-elastic-plastic behavior of material model

The initial yield, σ_0, and plastic hardening modulus, E_p, are temperature-dependent,

$$E_p(\theta) = \frac{E_t(\theta)E(\theta)}{E(\theta) - E_t(\theta)} \tag{8}$$

and ε^p_{eff} is the effective plastic strain

$$\varepsilon^p_{eff} = \int_0^t \sqrt{\frac{2}{3}\dot{\varepsilon}^p_{ij}\dot{\varepsilon}^p_{ij}}\,dt \tag{9}$$

The plastic strain rate tensor is computed by formula

$$\dot{\varepsilon}^p_{ij} = \dot{\varepsilon}_{ij} - \dot{\varepsilon}^e_{ij} - \dot{\varepsilon}^\theta_{ij} \tag{10}$$

where the thermal strain rate tensor is written in terms of the coefficient of thermal expansion α as

$$\dot{\varepsilon}^\theta_{ij} = \alpha\dot{\theta}\delta_{ij} \tag{11}$$

In the implementation of this material model, the elastic co-rotational stress rate tensor is computed as

$$\sigma^\nabla_{ij} = C_{ijkl}\left(\dot{\varepsilon}_{kl} - \dot{\varepsilon}^\theta_{kl}\right) + \dot{\theta}_{ij}d\theta \tag{12}$$

where C_{ijkl} is the temperature-dependent elastic constitutive matrix, and

$$\dot{\theta}_{ij} = \frac{dC_{ijkl}}{d\theta}C^{-1}_{klmn}\dot{\sigma}_{mn} \tag{13}$$

The stress tensor is updated elastically as

$$\sigma_{ij}^{*} = \sigma_{ij}^{n} + \sigma_{ij}^{\nabla} \Delta t \tag{14}$$

where σ_{ij}^{*} is the trial stress tensor, σ_{ij}^{n} is the stress tensor from the previous time step, and Δt is the incremental time.

Let s_{ij}^{*} represent the trial elastic deviatoric stress tensor at state n+1

$$s_{ij}^{*} = \sigma_{ij}^{*} - \frac{1}{3}\sigma_{kk}^{*}\delta_{ij} \tag{15}$$

Define the yield function:

$$\varphi = \frac{3}{2} s_{ij}^{*} s_{ij}^{*} - \sigma_y^2(\theta) = \Lambda^2 - \sigma_y^2(\theta) \begin{cases} \leq 0 \text{ for elatic or neutral loading} \\ > 0 \text{ for plastic hardening} \end{cases} \tag{16}$$

For plastic behavior, the stress deviatoric tensor is scaled back by factor f_s

$$s_{ij}^{n+1} = f_s s_{ij}^{*} \tag{17}$$

where

$$f_s = \frac{\sigma_y}{\sqrt{\frac{3}{2} s_{ij}^{*} s_{ij}^{*}}} \tag{18}$$

and plastic strain is updated by increment

$$\Delta \varepsilon_{eff}^{p} = \frac{(1 - f_s)\sqrt{\frac{3}{2} s_{ij}^{*} s_{ij}^{*}}}{G + 3E_p} \tag{19}$$

Several erosion criteria that are independent of the material models are available. In this study, the criterion of the total effective strain at failure is applied by formula

$$\varepsilon_{eff} = \int_0^t \sqrt{\frac{2}{3} \dot{\varepsilon}_{ij} \dot{\varepsilon}_{ij}}\, dt \geq \overline{\varepsilon}_{eff}^{\max} \tag{20}$$

and once it is satisfied, the element is deleted from the calculation.

3. Numerical model

The tensile tests were carried out at ambient temperature for standard samples with a circular cross section. The dimensions of the samples were assumed in accordance with the guidelines of PN-EN ISO 6892-1: 2010 [7] and are shown in Figure 3.

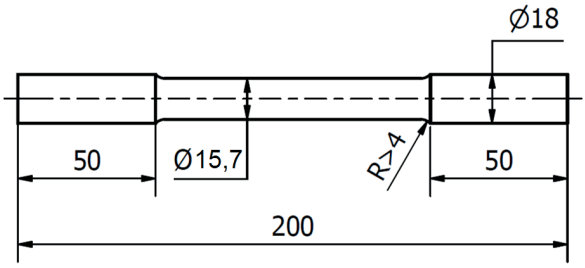

Fig. 3. The scheme of a sample for quasi-static tension tests at ambient temperature

The samples were made of stainless steel 41Cr4, which has the elastic-plastic characteristic. The tests were performed until the failure of the samples.

The three-dimensional models of the samples were created using MSC.Patran and Ls PrePost programs. The Ls-Dyna program was used for calculations. Numerical analyses were performed with the algorithm of thermo-mechanical coupling, in which it was assumed that plastic work is converted into heat in 95% consumed into the heat flux.

The model consisted of 73,720 three-dimensional elements of ELFORM1 type (which were described above). The minimum size of the edge of the element was 0.5 mm. In both models, the same mechanical boundary conditions were adopted. The nodes on the surface of the left grip were deprived of all degrees of freedom. Tensile forces were generated by displacement of the nodes on the right grip. The numerical model and scheme describing the mechanical boundary conditions are shown in Figure 4.

Thermal-mechanical properties of the material as a function of temperature were introduced in the form of the curves shown in Figure 5. Whereas, the effective strain at failure material was equal to 0.36 at a temperature of 100°C.

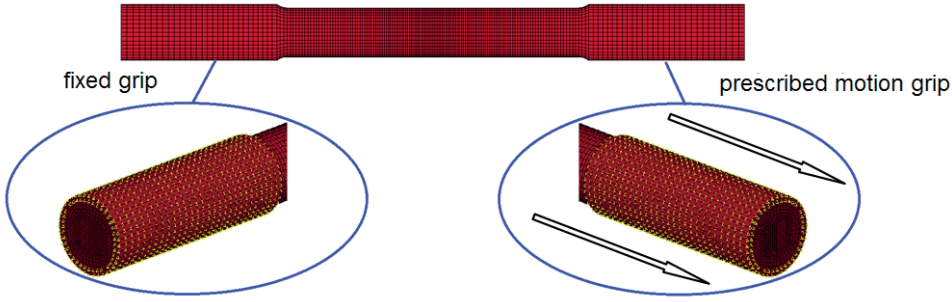

Fig. 4. The numerical model of the sample for tensile and scheme describing boundary conditions

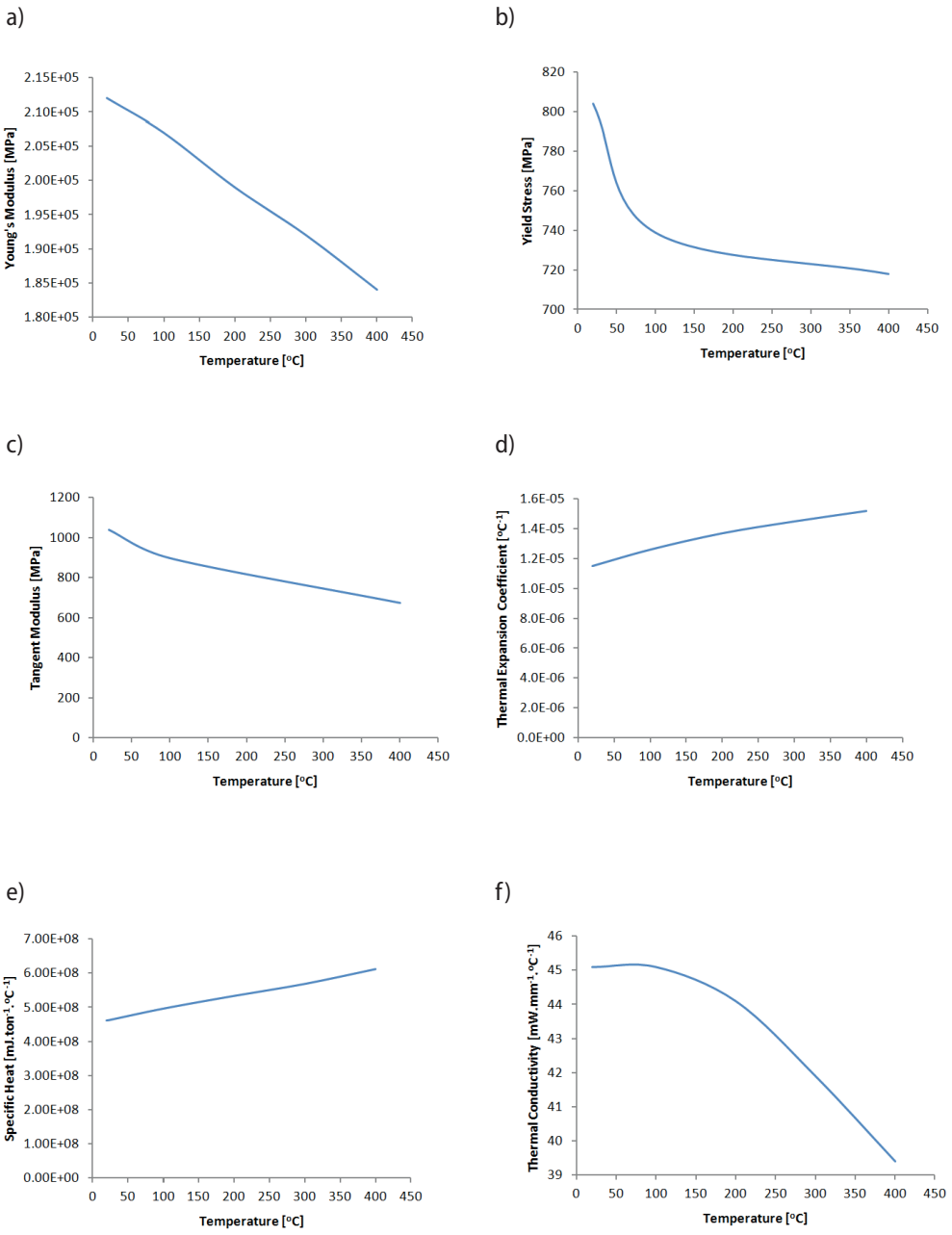

Fig. 5. Thermal-mechanical properties of the material as a function of temperature: a) Young's modulus; b) yield stress; c) tangent modulus; d) thermal expansion coefficient; e) specific heat; f) thermal conductivity

Two methods of mapping the thermal boundary conditions were analyzed. In each case, all nodes are assigned with an initial temperature of about 27°C. In the first model, it was assumed that the boundary conditions were perfectly adiabatic due to the short duration of the tensile test. In the second model, an additional thermal contact was mapped in the field of grips (Fig. 6), with the jaws of the INSTRON 8802 machine using the *CONTACT_SURFACE_TO_SURFACE card. The coefficient of the thermal conductivity through contact was 45.1 mW·mm^{-1}·C^{-1}.

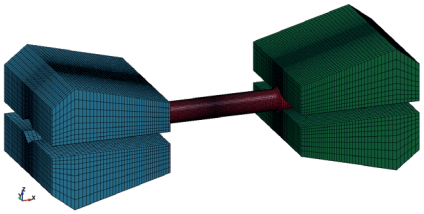

Fig. 6. The scheme of mapping the thermal contact between the sample and jaws of the machine

Figures 7 and 8 show the maps of temperatures and plots of temperature vs. time at the position of the appearance of the neck, obtained as a result of numerical analyses for both models.

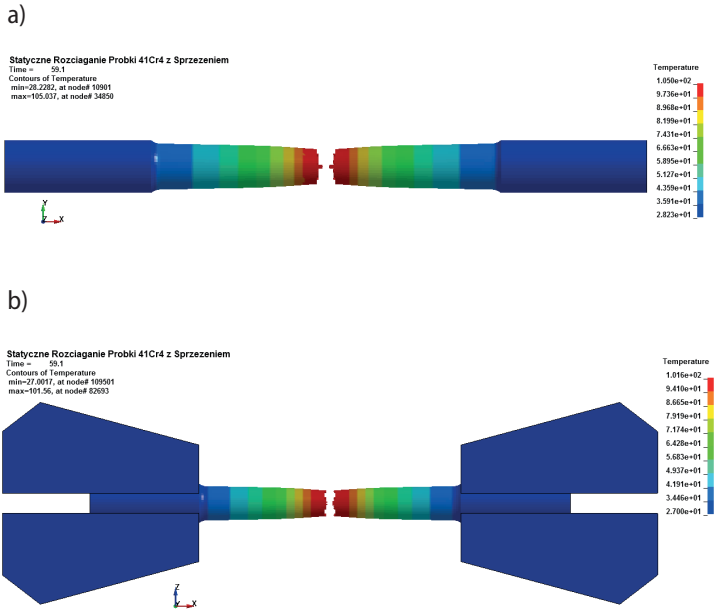

Fig. 7. Distribution of temperature at destruction of the samples: a) model adiabatic; b) model with heat contact

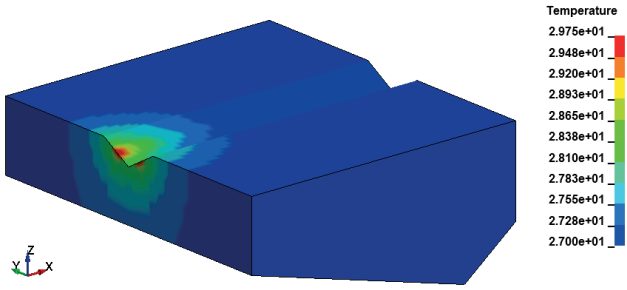

Fig. 8. The temperature distribution on the surface of the jaw at the time of failure

4. Numerical model validation

All of the results were compared with the results from the experimental studies. The tests were carried out at an ambient temperature on the Instron 8802 testing machine with a hydraulic drive. In front of the stand for static tests, thermal imaging camera FLIR SC 6000 was mounted in order to register the temperature distribution on the surface of the sample under tension. The test stand and photo of the samples are shown in Figure 9.

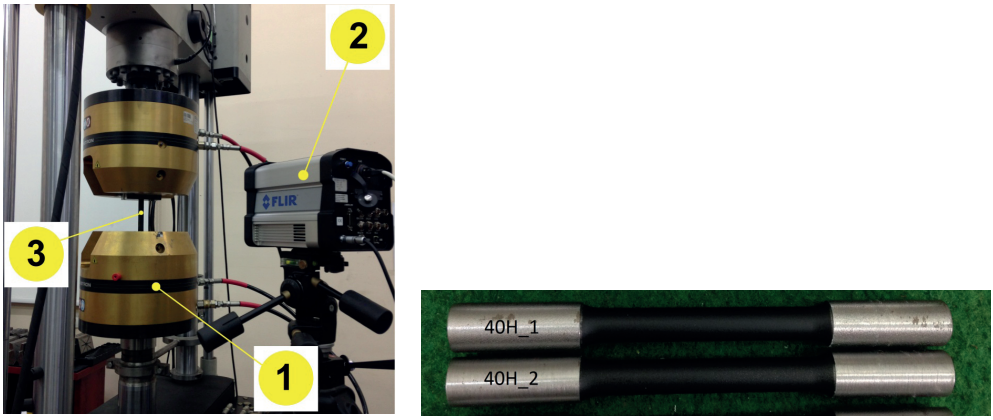

Fig. 9. The test with an infrared camera and the prepared samples: 1) testing machine INSTRON 8802; 2) infrared camera FLIR SC 6000; 3) sample

The studies were conducted for samples made of 41Cr4 chromium steel for quenching and tempering (surface hardening). The essential tests were preceded by tests on material emissivity.

A comparison of the results obtained from both the experiment and simulation are presented in Table 1 and Figure 10.

Table 1. Summary of the results from the experimental tests and numerical simulations for 41Cr4 alloy

No.	Experiment	Time [s]	Simulation FEM	Difference Δ°C	Correction Δ°C	Δ%
1.	Max. temp. = 104°C	60	Max. temp. = 105°C	+1	+1	1%

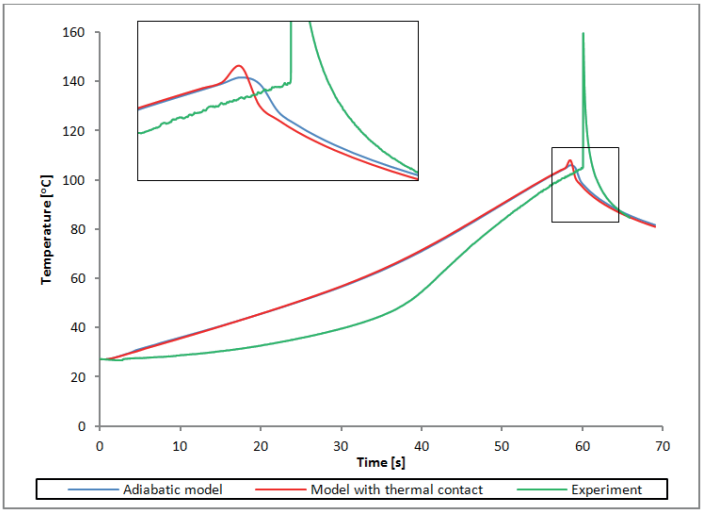

Fig. 10. Comparison of the results obtained from the experiment and from the simulation

The conducted analyses show that the applied FEM model is correct and the obtained results are consistent with the experience. Divergence of the maximum temperature for 41Cr4 alloy results from material data (that is not very accurate) taken from the literature, and it concerns the scope of intensive plastic deformation before failure.

The graph presented in Figure 10 shows that, in addition to the results of numerical simulations performed using thermo-mechanical coupling, a point can be observed where a sharp temperature increase occurs just before the failure of the rod.

It was also shown that the numerical simulations on the reliability of the results are also affected by the introduction of appropriate thermal boundary conditions. The divergence shown in Figure 10 may result from an inaccurate material model used in the model as well as from the accuracy of the conducted experimental tests resulting from the technical limitations of the equipment used.

The peaks on the graph shown in Figure 10 occur at the time of failure of the material at high speed and are instantaneous in this model approach (the high strain rate compared to the average of the sample and thermo-mechanically transient state).

5. Summary

The performed tests and numerical simulations provide a global response to the impact of thermo-mechanical coupling on the final result of a solution of the strength problem. Considerations related to the thermo-mechanical effects of coupling are important in the design of technological processes. They allow a better assessment of the energy demand for accomplishing this goal. Taking into account the effects of the influence of temperature on physical properties and the actual characteristics of the material in the analysis of engineering structures loaded mechanically and thermally enables the construction design and technological processes to be more efficient; that is, better in terms of strength, more economical, and more secure.

References

[1] Kleiber M., Kowalczyk P.: Wprowadzenie do nieliniowej termomechaniki ciał odkształcalnych. IPPT PAN, Warszawa 2011

[2] Niezgoda T.: Numeryczna analiza wybranych zagadnień termomechaniki. WAT, Warszawa 1992

[3] Oden J.T., Bhandari D.R., Yagawa G., Chung T.J.: A New Approach to the Finite Element Formulation and Solution of a Class of Problems in Coupled. Nuclear Engineering and Design, 24 (1973), 420–430

[4] Argyris J.H., Vaz L.E., William K.J.: Integrated Finite Element Analysis of Coupled Thermoviscoplastic Problems. Journal of Thermal Stresses, 4 (1981), 121–153

[5] Shapiro A.B.: TOPAZ3D – A Three Dimensional Finite Element Heat Transfer Code. University of California, Lawrence Livermore National Laboratory, Report UCID-20481, 1985

[6] LS-DYNA Theory Manual, Livermore Software Technology Corporation, 1992–2014

[7] PN-EN 10002-1+ACI:1998, Metale. Próba rozciągania. Metoda badania w temperaturze otoczenia